Review

TiO$_2$-based materials for photocatalytic hydrogen production

Gian Luca Chiarello, Maria Vittoria Dozzi, Elena Selli[*]

Dipartimento di Chimica, Università degli Studi di Milano, Via Golgi 19, I-20133 Milano, Italy

Abstract

Hydrogen, the cleanest and most promising energy vector, can be produced by solar into chemical energy conversion, either by the photocatalytic direct splitting of water into H$_2$ and O$_2$, or, more efficiently, in the presence of sacrificial reagents, e.g., in the so-called photoreforming of organics. Efficient photocatalytic materials should not only be able to exploit solar radiation to produce electron-hole pairs, but also ensure enough charge separation to allow electron transfer reactions, leading to solar energy driven thermodynamically up-hill processes. Recent achievements of our research group in the development and testing of innovative TiO$_2$-based photocatalytic materials are presented here, together with an overview on the mechanistic aspects of water photosplitting and photoreforming of organics. Photocatalytic materials were either i) obtained by surface modification of commercial photocatalysts, or produced ii) in powder form by different techniques, including traditional sol gel synthesis, aiming at engineering their electronic structure, and flame spray pyrolysis starting from organic solutions of the precursors, or iii) in integrated form, to produce photoelectrodes within devices, by radio frequency magnetron sputtering or by electrochemical growth of nanotube architectures, or photocatalytic membranes, by supersonic cluster beam deposition.

Key words: Photocatalytic H$_2$ production; Photo steam reforming; Flame spray pyrolysis; nanotubes; Noble metal nanoarticles; Photocatalytic devices

* Corresponding author. Tel: +39 02 503 14237; Fax: 39 02 503 14300; E-mail: elena.selli@unimi.it.

1. Introduction

Hydrogen is widely considered the clean energy vector of the future and technologies of energy production from hydrogen, e.g. fuel cells and internal hydrogen combustion engines, are already mature. However, hydrogen production and storage remain the main problems. In fact, hydrogen production is still based on fossil raw materials, its most important industrial production route consisting in the catalytic steam reforming of hydrocarbons, with water electrolysis contributing to only a few percent of the global production. Steam reforming implies gaseous hydrocarbons treatment with steam at high pressure and high temperature and is highly endothermic, i.e. heat must be supplied for the reaction to proceed, which is usually provided by the combustion of part of the feed stock, with a consequent decrease of the net yield of the whole process.

The great concern about global climate changes, related to the exploitation of fossil fuels, and the urgent need for alternative, environmentally friendly energy sources, led renewed, extensive attention to the photocatalytic production of hydrogen, either by the direct splitting of water into hydrogen and oxygen or by reforming of organic compounds, and in particular of biomass, on metal oxide semiconductors [1–4]. This latter process represents a sustainable option for the future energy economy.

Although a large number of materials potentially suitable for photocatalytic hydrogen production have been explored in recent years, including a variety of semiconductor oxides [5] and mixed metal oxide semiconductors, also with rather complex structure [6–10], as well as sulphides [11], nitrides [12], oxysulphides [13], and oxynitrides [14], titanium dioxide still remains the benchmark photocatalytic material [15–17], due to its peculiar intrinsic properties, particularly for hydrogen production, if its surface is modified by noble metal nanoparticles (NPs) deposition [18,19] or by grafting of metals [20,21]. Indeed, by this way one of the main issues concerning the use of semiconductors as photocatalysts, i.e. the separation of photogenerated charge carriers, can be overcome, the Fermi level of noble metals usually being lower in energy than the semiconductor conduction band energy. Thus, electrons photopromoted in the semiconductor conduction band can migrate to the noble metal NPs, whereas photoproduced holes remain in the semiconductor valence band. The other important issue related to the use of TiO_2 as photocatalyst in solar energy conversion, i.e. the fact that it absorbs only a limited fraction of the most energetic portion of the solar spectrum, is still far from being overcome, though several different approaches have been attempted to increase TiO_2 photoactivity in the visible region, e.g. by doping it with *p*-block elements [22], but the solution might possibly be found only by employing different semiconductor oxides.

Besides by noble metal nanoparticles deposition on TiO_2, the rate of photocatalytic hydrogen production is further increased in the presence of compounds (e.g. methanol [23–26], ethanol and glycerol) able to act as efficient hole scavengers and to fill them more readily than water itself in the photocatalytic splitting of pure water. Of course, also organics deriving from renewable sources, such as biomasses, may be profitably employed as hole scavengers. Furthermore, photocatalytic hydrogen production has been mainly investigated in water suspension, with rare examples of investigation of the vapour phase photo-steam reforming reaction [23,27,28].

In recent years we performed a systematic investigation on hydrogen production by photocatalytic steam reforming, mainly employing methanol as a volatile and simple organic electron donor acting as a sacrificial reagent able to combine with photoproduced holes, in a model reaction of photocatalytic hydrogen formation from renewable sources. Photocatalysts home prepared by different techniques, also containing noble metal nanoparticles, were employed in this type of investigation and a systematic analysis of the methanol content-dependent mechanistic aspects of the reaction has been performed. TiO_2-based materials constituting the photoactive layer of the photoelectrodes employed in a two compartment cell for separate hydrogen and oxygen evolution from water solutions have also been successfully prepared and tested under different conditions. A critical overview of our main results is presented here.

2. Testing photocatalysts in powder form

2.1. Photocatalytic reactor for hydrogen production tests

We first performed photocatalytic activity tests in hydrogen evolution employing TiO_2-based photocatalyst powders dispersed in illuminated aqueous suspensions [29]. The photoreactor consisted in a magnetically stirred cylindrical quartz vessel, inserted in a closed stainless steel circulating system, in which an inert gas (nitrogen) was continuously fluxed by means of a bellow pump. The analysis of the species evolved from the aqueous suspension under irradiation and accumulated in the gas phase was performed by gas chromatographic analysis, after calibration. Hydrogen evolved at almost constant rate, except for a slight initial lower rate within the first 2 h. The light was an iron halide mercury arc lamp, emitting in the 330–450 nm wavelength range. However, when investigating the effects of magnetic stirring and bubbling of the recirculating gas, the existence of mass transfer effects was established. In fact, the rate of hydrogen production increased when the system was stirred, as expected, and almost doubled when the recirculating gas was bubbled through the gas porous septum, as a consequence of the fact that hydrogen photoproduced on the photocatalyst surface has to desorb and diffuse through the liquid phase before reaching the gas phase. Therefore all preliminary photocatalytic tests were carried out under

3

strictly controlled, constant rate magnetic stirring and gas phase bubbling into the irradiated suspension. Furthermore, difficulties were encountered in the repetition of the photocatalytic runs employing an already used photocatalyst suspension, because the photocatalyst powder partially deposited on the reactor walls from the stirred suspension during the run and could not be fully recovered and exploited in subsequent runs.

For these main reasons the irradiated photoreactor containing the stirred photocatalyst suspension was substituted with a vapour phase reactor consisting of Plexiglas cell, hosting the same amount of photocatalyst contained in the suspensions, deposited on fine quartz grains. A sketch of the laboratory scale apparatus and of the automated sampling and detector system employed in all our subsequent test studies is shown in Fig. 1; a full description of the apparatus can be found elsewhere [30].
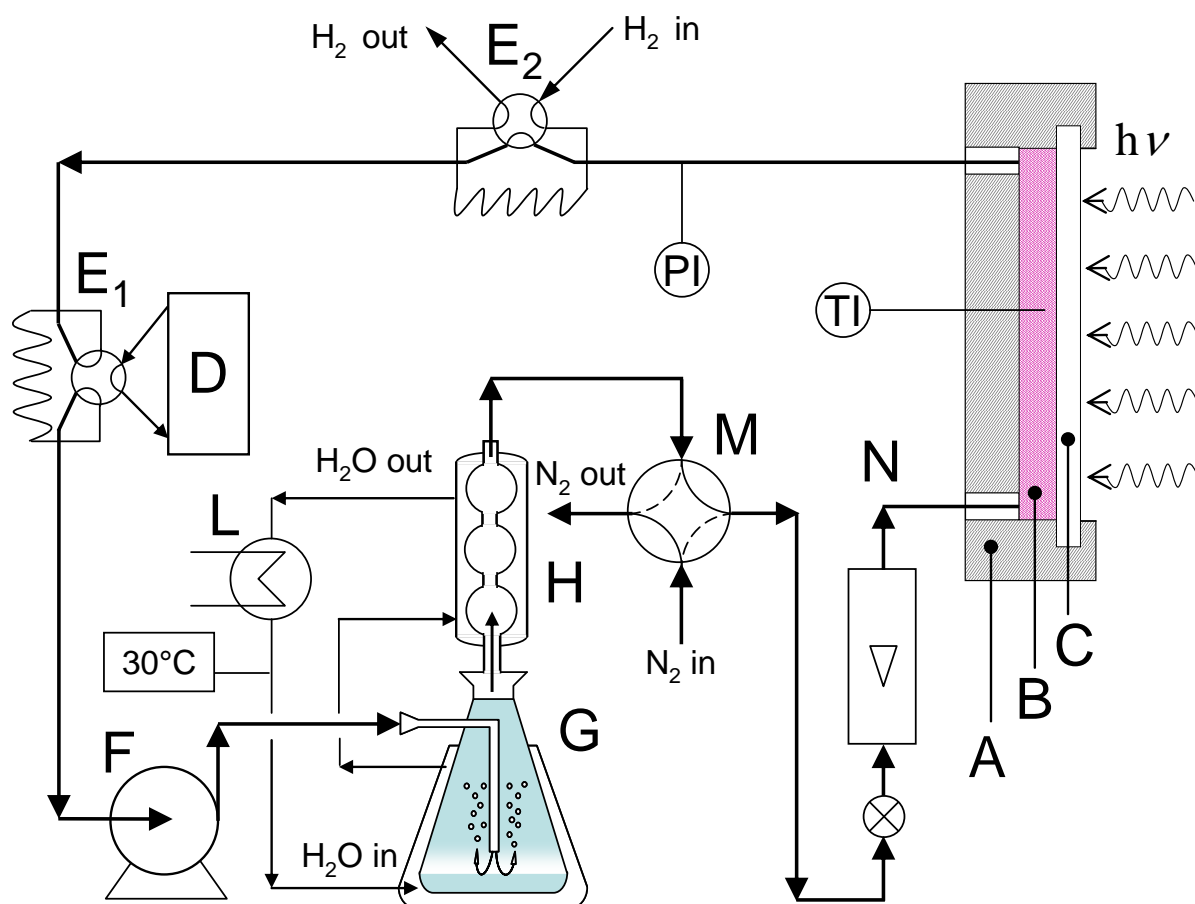

Fig. 1. *Sketch of the experimental set up for vapour phase photocatalytic activity measurements. (A) Plexigas photoreactor; (B) photocatalysts bed; (C) Pyrex-glass window; (D) detector (gas chromatograph or quadrupolar mass spectrometer); (E$_1$, E$_2$) six ways sampling valves; (F) bellow pump; (G) thermostated bubbler; (H) refrigerator-condenser; (M) four ways ball valve (dotted line: position for pre-flushing with inert gas; solid line: position for gas-phase recirculation; (L) thermostat; (N) gas flow meter; TI and PI: temperature and pressure indicators. Reprinted from Ref. [30], Copyright (2009), with permission from Elsevier.*

During irradiation the reactor temperature slightly increased above room temperature. Also the pressure, ca. 1.2 bar at the beginning of the test, increased during irradiation, as a consequence of hydrogen accumulation in the gas phase. The bubbler reservoir was filled with water, in water photosplitting tests, or with a methanol in water solution, containing 20 vol% methanol, corresponding to a methanol molar fraction $x = 0.1$, under standard photo steam reforming conditions. The gas phase generated by bubbling nitrogen in the reservoir, kept at 30 °C, was then fed to the catalyst bed in the photoreactor and continuously recirculated at constant rate. Any trace of oxygen was removed prior to the runs by thoroughly flushing the whole set up with saturated nitrogen, in the absence of irradiation. The original iron halide mercury arc lamp was later substituted with a 300 W Xe arc lamp, also operated with different cut off filters. The irradiation intensity on the reactor was frequently measured with an optical power meter equipped with a thermal power sensor.

2.2. *Photocatalytic hydrogen production over flame spray pyrolysis synthesised TiO₂*

The photocatalytic hydrogen production from water splitting and methanol reforming was first investigated employing a set of titanium dioxide and gold-modified titanium dioxide photocatalysts prepared by flame spray pyrolysis (FP) in a single step [29], a technique which proved to be very effective for the synthesis of nanosized and noble-metal modified materials, characterized by high surface area and crystallinity, and excellent noble metal dispersion [31–33]. The tested materials were home prepared through an optimized FP synthesis, which is based on the solvent evaporation and burning of an organic solution containing the titanium precursor and eventually the noble metal precursor, followed by nucleation, condensation and aggregation of flame-made oxide nanoparticles. In particular we focused on the effects that the organic solvent and operating conditions may have on the physicochemical properties of the produced powders in relation to their photocatalytic activity in water splitting and methanol reforming.

All FP-made photocatalysts consisted of a mixture of anatase and rutile crystal phases, in different percent amounts. Their specific surface area (SSA) was found to linearly decrease with increasing the combustion heat of the organic solvent/fuel employed in their synthesis [29]. When a xylene/pyridine mixture was employed as solvent, the highest anatase content, crystallinity and SSA were attained, which were not affected by the presence of 1% gold NPs. HRTEM analysis showed a bimodal distribution of crystalline particles, with a majority of smaller (5-10 nm sized) particles accompanied by some bigger (100-500 nm) particles. Very small and well dispersed, 1-2 nm sized gold or platinum NPs [34] can be evidenced in Au- or Pt-containing FP-TiO₂, as shown in the images reported in Fig. 2.

5
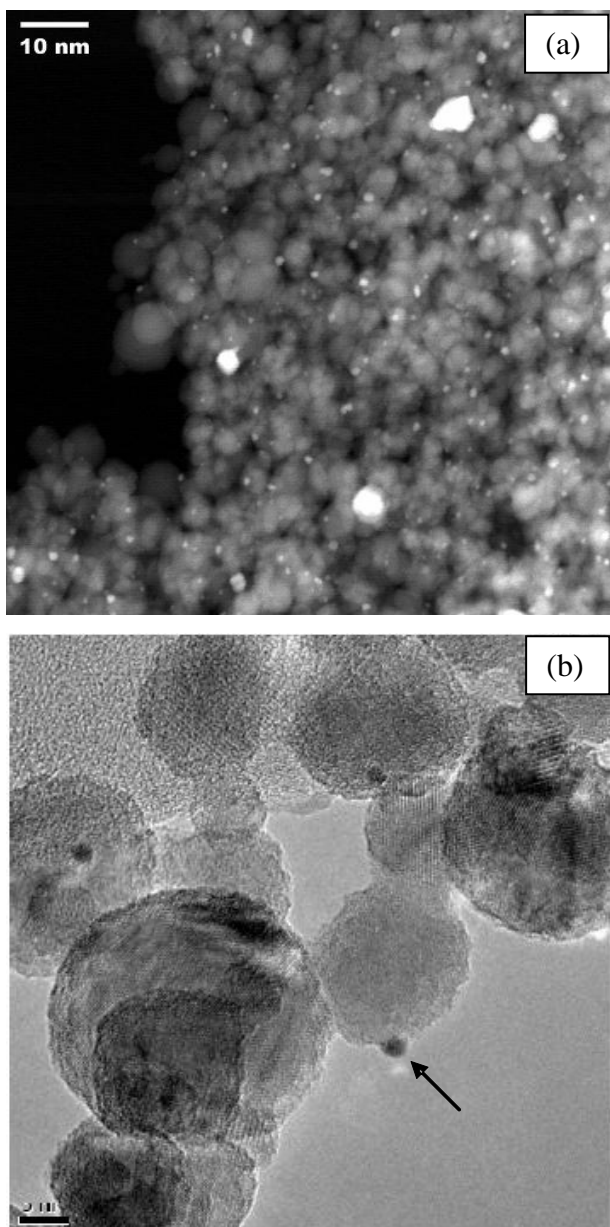
Fig. 2. *(a) STEM-HAADF image of flame-made TiO$_2$ containing 1% Au nanoparticles, appearing as bright dots. (b) HRTEM image of FP-0.5%Pt/TiO$_2$; the arrows point to a noble metal nanoparticle. Adapted from Ref. [29], Copyright (2008), and from Ref. [34], Copyright (2010), with permission from Elsevier.*

With all investigated materials hydrogen was found to evolve from water suspensions at constant rate under irradiation, with a slight initial decrease in rate usually occurring within the first 2 h. This may be ascribed to the presence of some residual carbon-containing species on the photocatalysts, acting as more efficient hole scavengers with respect to water molecules, and thus ensuring higher initial hydrogen production up to their complete oxidation.

Bare TiO$_2$ photocatalysts exhibited low activity in water photosplitting, with FP-made TiO$_2$ samples performing better than benchmark commercial P25 TiO$_2$ [29]. Much better results were

obtained over gold-containing photocatalysts, due to the beneficial effect of noble metal NPs, able to capture the electrons photopromoted in the semiconductor conduction band. In particular, a FP-made sample containing 1% gold NPs proved to be the most active photocatalyst, with a photocatalytic activity in hydrogen evolution higher with respect to that of a photocatalyst prepared from P25 by 1% gold NPs deposition from a *tetrakis*(hydroxymethyl) phosphonium chloride-stabilized gold NPs solution [35]. The rate of hydrogen production, r_{H2}, obtained with both FP and commercial photocatalysts increased by one order of magnitude upon 1% gold NPs addition, and the more active was the bare photocatalyst, the more active was the gold-modified photocatalyst obtained through the same production route [29].

A significantly higher hydrogen production rate was attained from water suspensions containing 6 vol% methanol. Methanol acts as an efficient hole scavenger, thus decreasing the electron-hole recombination rate and making conduction band electrons more readily available for H^+ reduction. The rate of hydrogen production also increased with increasing the anatase content of the materials, with pure commercial rutile being by far the less performing material, and with increasing the SSA of the photocatalytic materials, as expected. Also the amount of surface defects were found to play a role, possibly acting as recombination centres of the photogenerated electron-hole pairs.

Finally, an outstanding increase in the rate of hydrogen production (r_{H2}) was attained in methanol reforming with a Au-containing FP-made photocatalyst. The activity was so high that purging with N_2 was required every 2 h, to prevent overpressure. Successive irradiation cycles were thus performed with the same photocatalyst bed, with N_2 purging in the dark after each irradiation cycle. No induction period in hydrogen evolution was observed in this case, but only a slight decrease in hydrogen production rate in successive cycles, as shown in Fig. 3, and a r_{H2} value ca. 30 times higher than with the Au-free FP-photocatalyst. The so obtained high r_{H2} values are a direct consequence of the simultaneous beneficial effects of segregation of photopromoted electrons by gold NPs and scavenging of photoproduced holes by methanol [29]. A further 30% higher reaction rate was attained with the vapour phase reactor, i.e. in the absence of liquid-phase mass transfer rate limitations [30], up to an apparent photon efficiency of 6.3%.
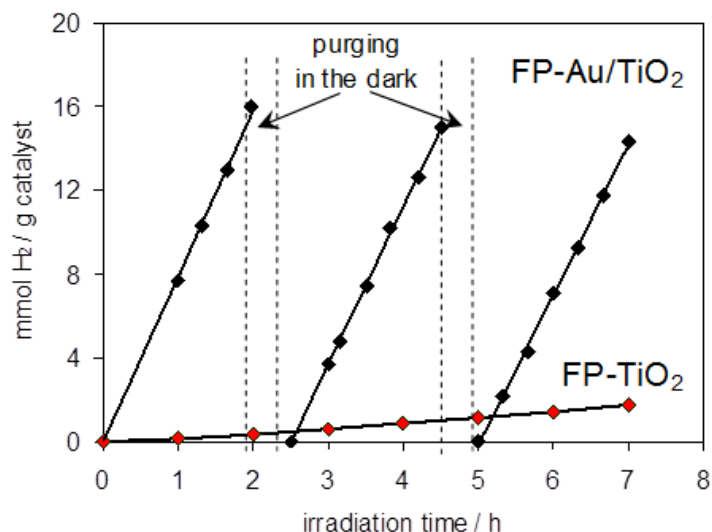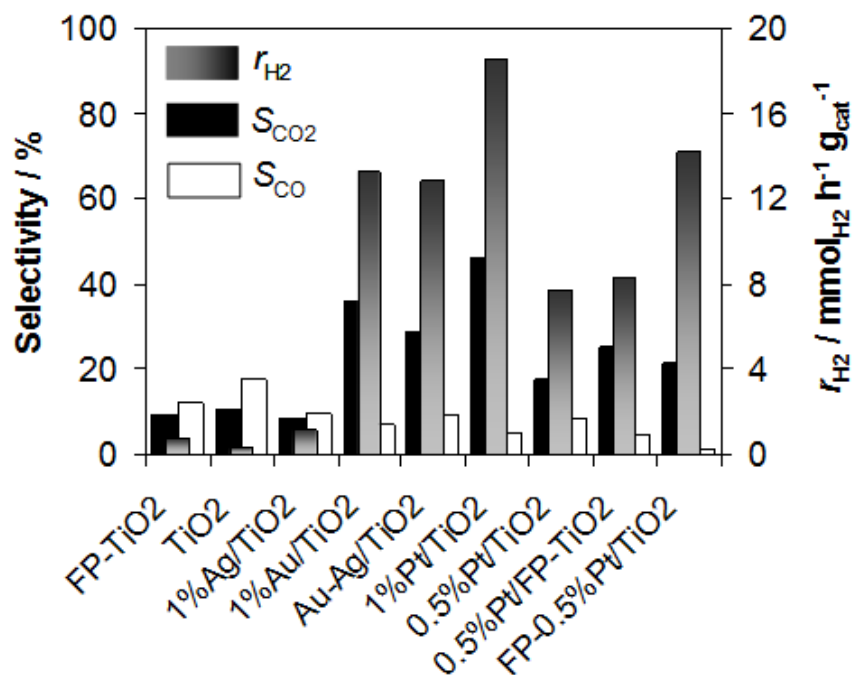
Fig. 3. *Hydrogen production from photocatalytic methanol reforming on a FP-made (red) and a gold-containing FP-made (black) TiO₂ photocatalyst. Adapted from Ref. [29], Copyright (2008), with permission from Elsevier.*

2.3. Effects of noble metal NPs on TiO₂ and of the TiO₂ phase composition

A systematic investigation was then performed on hydrogen production from photocatalytic steam reforming of methanol, employing a series of noble metal (NM) containing TiO_2 photocatalysts, either synthesized by FP, or obtained by the deposition of preformed NM NPs on TiO_2 [34,36]. The overview, reported in Fig. 4, of the hydrogen production rate and selectivity values to CO and CO_2 obtained with the investigated photocatalysts in contact with vapours produced from a 20 vol% methanol in water solution outlines that silver is the less effective co-catalyst, with only a four-fold r_{H2} increase with respect to r_{H2} on bare P25 TiO_2, whereas r_{H2} increased by 37 and 52 times when the same amount of gold or platinum NPs, respectively, were present on TiO_2.

Fig. 4. *Rate of hydrogen production, r_{H2}, in photocatalytic methanol reforming and percent selectivity to CO_2 and to CO obtained with a series of metal containing TiO_2 photocatalysts. Those prepared by flame spray pyrolysis are indicated by FP. Reprinted from Ref. [34], Copyright (2010), with permission from Elsevier.*

The difference in the photocatalytic performance of the three metal co-catalysts was related to their work function values (Φ), i.e. the energy required to promote an electron from the Fermi energy level into vacuum. The larger is the difference between the metal work function and that of the TiO_2 support, the higher is the Schottky barrier [18], the electronic potential barrier generated by the band alignment at the metal–semiconductor heterojunction, with consequent increased efficiency of photopromoted electrons transfer and trapping by the metal, resulting in a higher r_{H2} value. For the 111 crystal plane of Ag, Au and Pt, $\Phi = 4.74$ eV, 5.31 eV and 5.93 eV, respectively, whereas $\Phi = 4.6–4.7$ eV for TiO_2 [34]. Consequently, Pt is a more efficient electron trapper than gold, in line with the higher photoactivity of Pt-modified TiO_2. By contrast, the Φ value of Ag, very close to that of TiO_2, suggests scarce electron transfer, resulting in less efficient charge separation and thus little improvement in the photocatalytic performance upon Ag addition to TiO_2.

The same trend was reflected by the selectivity to CO_2, S_{CO2}, in the series of photocatalysts containing 1% metal on P25 TiO_2 (see Fig. 4), 1%Pt/TiO_2 being the most selective photocatalyst, followed by 1%Au/TiO_2 and 1%Ag/TiO_2. Moreover, when considering the use of hydrogen to feed fuel cells, CO, being a well-known poison for the Pt-based catalysts in fuel cells, is the most undesired by-product. From the point of view of selectivity to CO, S_{CO}, bare TiO_2 is the less

performing photocatalyst, while NM deposition on TiO_2 was found to significantly increase S_{CO2} and decrease S_{CO}. Thus, a more efficient separation between photoproduced charge carriers in the photocatalyst leads to both more efficient reduction paths, mainly leading to H_2 production, and complete CH_3OH oxidation to CO_2 by valence band holes. Furthermore, a more than doubled r_{H2} value was attained by doubling the amount of Pt deposited on TiO_2 P25, from 0.5% and 1% (Fig. 4), and even more remarkable was the effect observed in S_{CO2} values, increasing from 17.5% to 46.4% [34].

The 0.5 wt%Pt-containing photocatalysts prepared either by deposition of preformed metal NPs on P25 TiO_2 (0.5%Pt/TiO_2) or on FP-TiO_2 (0.5%Pt/FP-TiO_2) exhibit very close photoactivity in hydrogen production, whereas the Pt-containing photocatalyst prepared by FP in one step (FP-0.5%Pt/TiO_2) exhibited an exceptionally higher performance, with an extremely low selectivity to CO (Fig. 4), possibly due to the lower Pt particle size and higher Pt dispersion on the TiO_2 surface, typical of flame made catalysts [29,34].

Concerning the possible effects on photoactivity of the different phases of titanium dioxide, our flame-made materials mainly consisted of a anatase phase, with a ca. 10% rutile content. Titanium dioxide notoriously may exist in the three main polymorphs anatase, rutile and brookite, displaying rather different physico-chemical properties. Anatase and rutile are the most easily encountered and investigated forms, because pure brookite is quite difficult to synthesize.

A systematic investigation was performed by us on the photocatalytic activity of the three TiO_2 polymorphs employing almost pure phase crystalline oxides in powder form, both naked and after deposition of fine platinum NPs on their surface from a colloidal solution [37]. In this study pure rutile was found to perform even better than anatase in hydrogen production from photocatalytic steam reforming, both in the presence and in the absence of Pt NPs on the photocatalyst surface, possibly due to the smaller band gap of rutile, which makes it able to absorb a larger fraction of the emission spectrum of the xenon lamp employed as irradiation source in the photocatalytic tests. Pure brookite modified by deposition of Pt NPs also proved to be an excellent photocatalyst for hydrogen production from methanol-water vapors [37].

The effect of noble metal nanoparticles deposition was investigated also with a series of fluorine-doped materials prepared by the sol-gel method in the presence of different amounts of NH_4F, used as a dopant source [38,39], and then calcined at 700 °C. The nominal dopant/titanium percent molar ratios were 5, 7 and 12; doped materials were labelled as D_X, with X referring to the nominal dopant/titanium percent molar ratio. A reference undoped material, labelled as R/TiO_2, was prepared by exactly the same synthetic route, in the absence of dopant. XPS analysis confirmed the

presence of both N and F, mainly in substitutional and surface forms, respectively, both increasing with increasing nominal dopant amount [39]. All bare photocatalysts, though calcined at 700 °C, consisted of almost pure anatase phase [40], confirming that doping inhibits the anatase into rutile phase transition, which is typically observed after annealing undoped titania at temperature above 600 °C. These doped materials were modified by 0.5 wt% gold or platinum NPs photodeposition, which was performed by irradiating aqueous suspensions containing $HAuCl_4$ or H_2PtCl_6 with a low pressure mercury arc lamp under nitrogen atmosphere [40].

As shown in Fig. 5, almost identical bell shaped photoactivity trends in photocatalytic hydrogen production were obtained for the naked, reference (R/TiO_2), Au- and Pt-modified doped titania photocatalysts series with increasing dopant content, with 5% NH_4F-doped TiO_2 always being the best photocatalysts within each series. This demonstrates that the electronic structure of the doped materials has a crucial role in determining the absorption features and the photoproduced charge separation and mobility within the doped photocatalyst oxide.
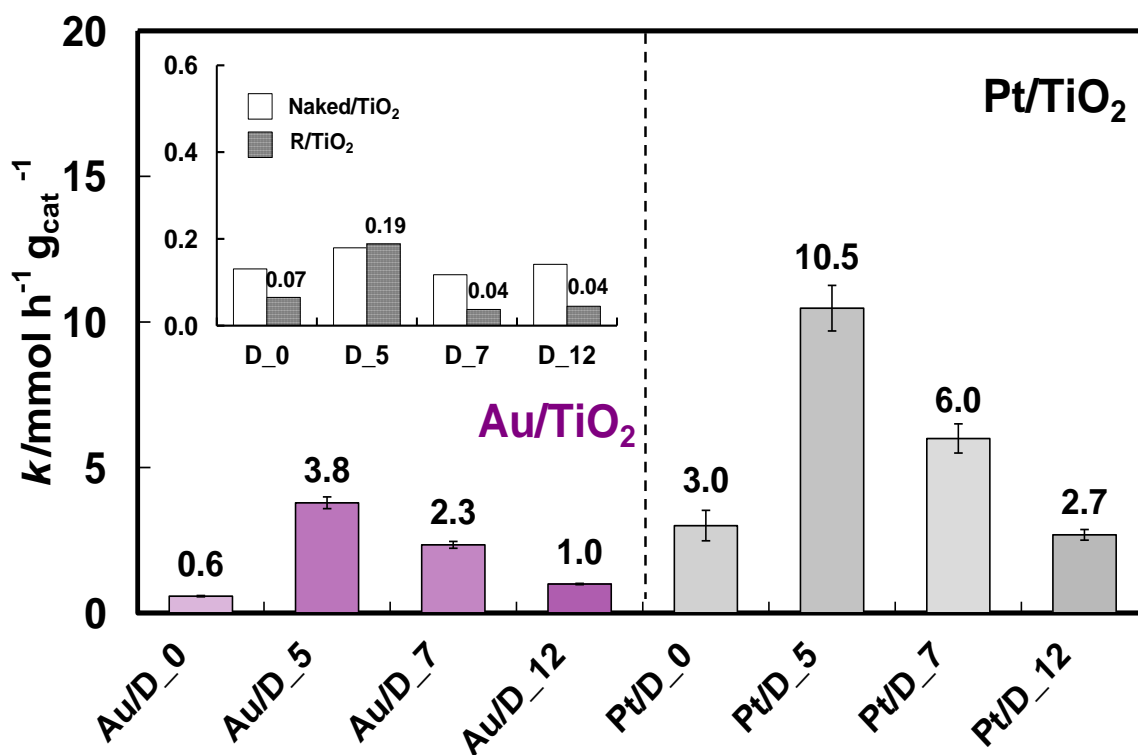

Fig. 5. *Zero order rate constants of hydrogen photocatalytic production and selectivity to CO_2 and to CO in the photocatalytic methanol reforming on naked and reference NH_4F-doped TiO_2 (DX series, upper inset) and on 0.5 wt% Au- or Pt-modified NH_4F-doped TiO_2. X indicates the nominal dopant/titanium percent molar ratio.*

11

On the other hand, the main role of the NM deposited on the doped TiO_2 material is limited to an increased efficiency of electron-hole separation by "capturing" the electrons photopromoted in the CB, platinum always being a more efficient co-catalyst than gold in ensuring this. However, the intrinsic efficiency in charge carrier photoproduction and separation is exclusively determined by the peculiar, intrinsic electronic features of these doped TiO_2 photocatalytic materials [40,41].

Most importantly, very intriguing synergistic effects in photoactivity induced by the simultaneous bulk and surface TiO_2 modification were outlined in hydrogen production for these NM-modified, doped TiO_2 materials, the increase of hydrogen production rate obtained with such materials with respect to that measured with the undoped naked material always being larger than the sum of the increases in hydrogen production rate obtained upon NM NPs deposition and upon doping TiO_2. This indicates that the peculiar electronic structure of TiO_2 obtained by doping it with fluorine, followed by calcination at 700 °C, contributes in increasing the electron transfer and charge separation effect occurring in the presence of surface NM NPs [40].

Fluorinated, nanostructured Pt-containing titania photocatalysts very effective in hydrogen production from methanol photocatalytic steam reforming were obtained also by FP in single step [42]. The introduction of fluoride in the solution to be burned during the synthesis, together with the short residence time of the growing oxide particles in the hottest zone of the flame, led to the formation of nanocrystals undergoing an anatase into rutile transformation shifted to slightly lower temperature as well as to a smaller anatase and rutile unit cell volume with respect to FP-made F-free TiO_2. As shown in Fig. 6, the highest hydrogen production rate (and highest carbon dioxide production from methanol reforming) was attained also in this case for a 5% nominal fluorine substitution for oxygen, whereas excessive fluorination was found to produce detrimental effects in both the surface and the bulk properties of FP-made TiO_2.
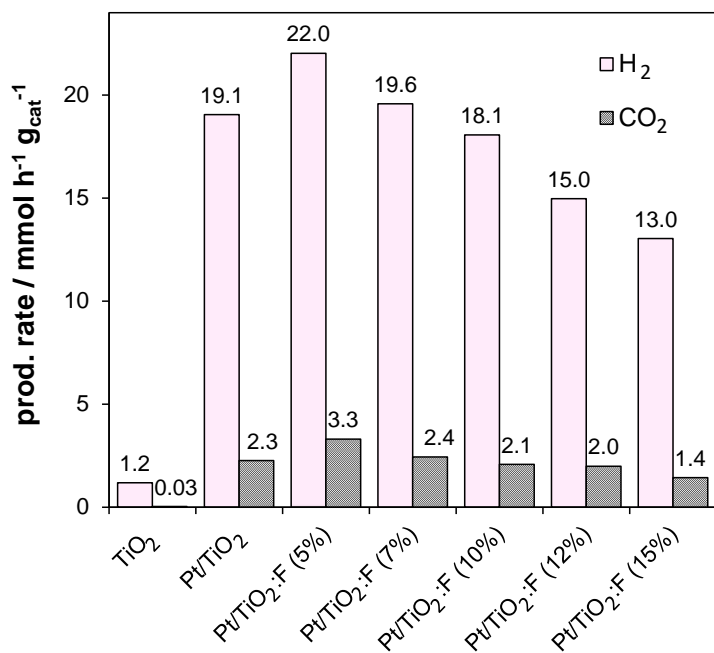
Fig. 6. *Effect of fluorine nominal content on the rates of H_2 and CO_2 production during photocatalytic methanol reforming over one step flame-made fluorinated Pt/TiO_2. Reprinted from Ref. [42], Copyright (2014), with permission from Elsevier.*

2.4. Mechanism of photocatalytic hydrogen production from methanol reforming

Besides the two main photoreaction products, i.e. hydrogen and carbon dioxide, also formaldehyde, carbon monoxide, dimethyl ether, methyl formate, acetaldehyde and traces of methane and ethane, as by-products, were detected during the photocatalytic steam reforming of methanol [34].

Fig. 7 displays the typical composition vs. time profiles of the recirculating gas during irradiation. The concentration of water and methanol (Fig. 7a) did not significantly vary under steady state conditions, due to their low percent conversion. The concentration of H_2, CO_2, CO and CH_4 (Fig. 7b) increased linearly with time because they accumulated in the recirculating gas phase, according to a pseudo-zero order rate law, whereas the concentration of formaldehyde, methyl formate, acetaldehyde and dimethyl ether (Fig. 7a and 7c) rapidly increased at the beginning of the runs and then remained almost constant in the gas phase, because they accumulated in the methanol-water liquid solution when the gas phase bubbled into it. Formic acid was never detected in the gas phase, very likely because its amount was below the detection limit, but it accumulated in the liquid solution, as confirmed by ionic chromatographic analysis at the end of the runs [34].

13
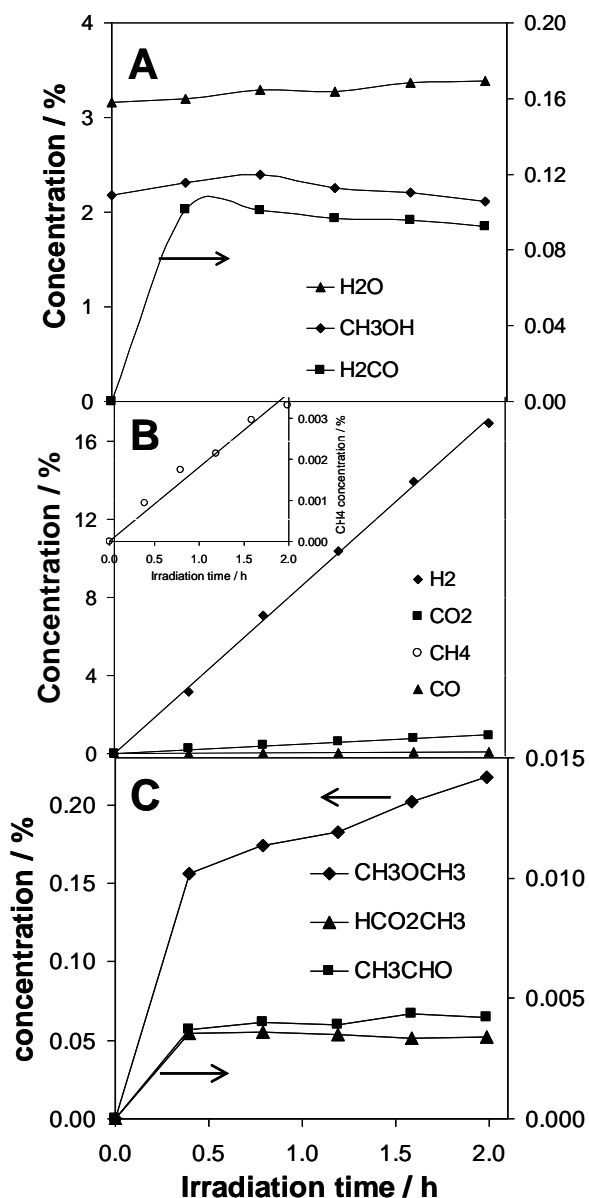
Fig. 7. *Typical gas phase composition during the photocatalytic methanol reforming tests. Reprinted from Ref. [34], Copyright (2010), with permission from Elsevier.*

In order to ascertain how the rates of products formation are influenced by the methanol/water molar ratio in the recirculating gas phase under irradiation and to discern the role of water in hydrogen production and methanol oxidation, a systematic investigation was performed by varying the methanol and water partial pressures. The rate of formation of the main reaction products was thus investigated with both the FP-0.5%Pt/TiO$_2$ (flame-made in a single step) photocatalyst and a 1.0 wt% gold NPs containing TiO$_2$ photocatalyst (labelled 1%Au/TiO$_2$), which was prepared by deposition of preformed, surfactant stabilized Au NPs on commercial P25 TiO$_2$, according to the reverse micelle method [43]. These two photocatalysts were fed with vapours in equilibrium with water/methanol liquid solutions, kept at 30 °C, containing different methanol molar fractions *x*

14

$(0.0045 \leq x \leq 1)$ [44]. The rates of hydrogen production, r_{H2}, and the selectivities to CO and to formic acid, S_{CO} and S_{HCOOH}, respectively, determined with the two photocatalysts as a function of the molar fraction x of methanol in the liquid phase are shown in Fig. 8.
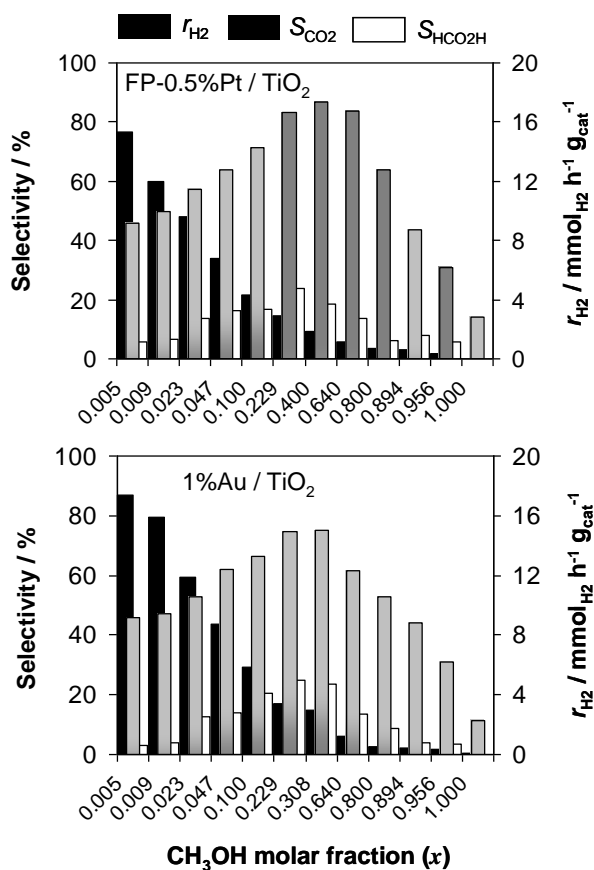

Fig. 8. *Hydrogen production rate (r_{H2}) and selectivity to CO_2 (S_{CO2}) and to formic acid (S_{HCOOH}) as a function of the methanol molar fraction x in the liquid solution in equilibrium with the gas mixture fed to the photoreactor. Reprinted from Ref. [44], Copyright (2011), with permission from Elsevier.*

At low x values the rate of hydrogen production r_{H2} was found to be lower than at high x values and both r_{H2} and S_{HCOOH} exhibit an asymmetric bell-shaped trend with a maximum located at $0.2 < x < 0.65$. Furthermore, the rate of CO_2 production and also S_{CO2} display a hyperbolic decay trend with increasing x, the maximum rate of carbon dioxide production being attained at high water to methanol molar ratios. Thus, as the partial pressure of methanol in the vapor phase increases, S_{CO2} decreases and formaldehyde becomes the main product of methanol oxidation. These results clearly evidence the crucial role of water in guaranteeing the attainment of complete oxidation in the vapor phase photoreforming of methanol under anaerobic conditions.

The sequence of photoinduced oxidation reactions occurring on the photocatalyst surface under steady state conditions is schematically represented in Fig. 9. Methanol and water adsorb competitively on the oxide surface, with the formation of surface hydroxyl and methoxy groups

15

[42]. Adsorbed methanol is then oxidized up to CO_2 on the photocatalyst surface, through formaldehyde and formic acid formation, as intermediate species. Under steady state conditions, the surface concentration of the intermediates is constant and a competition is established at each step between further oxidation of the adsorbed intermediate species and their desorption into the vapor phase. The higher is the desorption rate with respect to the oxidation rate, the higher is the accumulation rate of that intermediate in the gas phase and consequently the lower is the selectivity to CO_2.
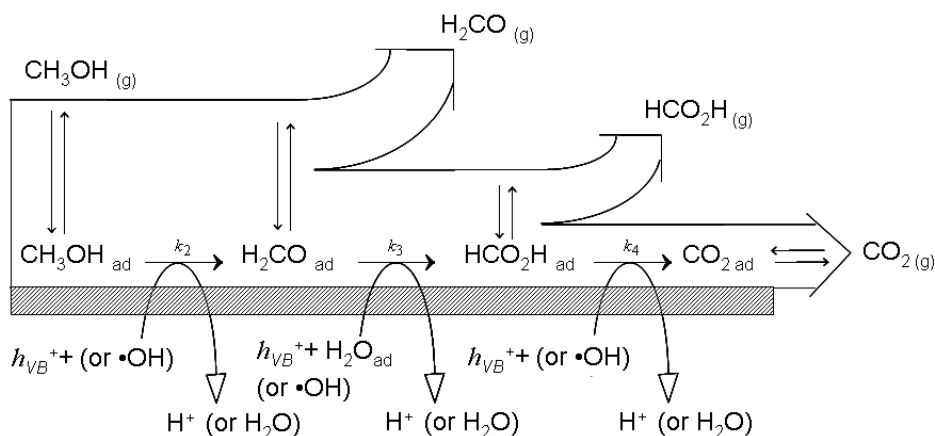

Fig. 9. *Reaction scheme of the photocatalytic vapour phase oxidation of methanol on the TiO₂ surface under steady state conditions. Reprinted from Ref. [44], Copyright (2011), with permission from Elsevier.*

Each oxidation step may proceed on the photocatalyst surface either by the direct interaction of the adsorbed organic species with valence band holes, or by an indirect path involving hydroxyl radical attack. Any $^{\bullet}$OH radical-mediated path implies water adsorption, which reacts with valence band holes, producing protons and reactive $^{\bullet}$OH radicals adsorbed on the photocatalyst surface. Each hole mediated oxidation step also produces H^+, and crucial is the diffusion of the so-produced protons over the titania surface towards the NM NPs, where photopromoted electrons accumulate under irradiation. Also note that formaldehyde oxidation can only proceed through hydroxyl radical attack, because H_2CO transformation into HCOOH requires an extra oxygen atom, which can only be provided by water, through a hydroxyl radical.

With this reaction scheme, which takes into account both the direct and the $^{\bullet}$OH radical mediated path at each oxidation step occurring on the photocatalyst surface, a final rate expression was obtained which was able to account for the CO_2 production rate decaying with increasing methanol molar fraction x (see Fig. 10), but not for the bell-shaped curves of formaldehyde and formic acid production rate vs. x. We thus concluded that water does not simply act as a source of $^{\bullet}$OH radicals,

16

but acts as a diffusion medium for protons produced on the titania surface at each oxidation step, which have to reach the NM where proton reduction yielding hydrogen occurs. By taking into account a third parallel reaction path, a so called water assisted path, with a rate increasing with increasing both methanol and water concentration, the bell-shaped behavior vs. x of formaldehyde and formic acid production rates could perfectly be accounted for [44].
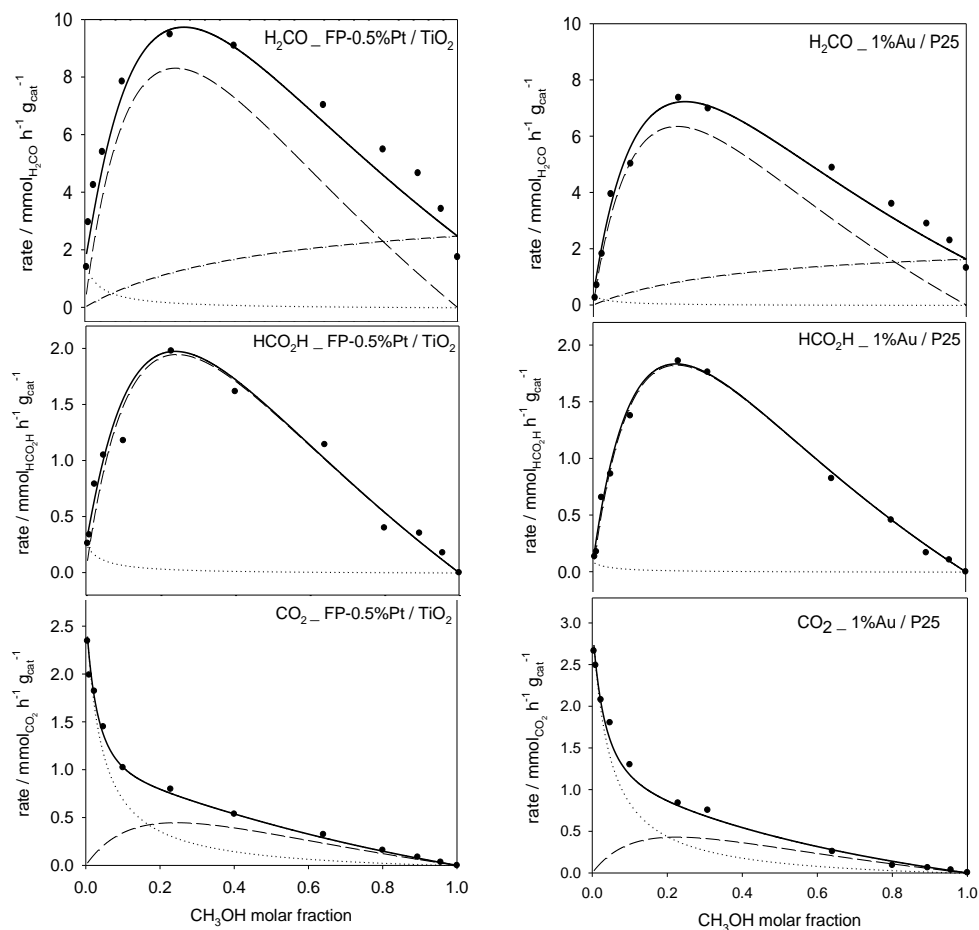

Fig. 10. *Rates of formaldehyde, formic acid and carbon dioxide production measured with the FP-0.5%Pt/TiO$_2$ (left panels) and 1%Au/TiO$_2$ (right panels) photocatalysts at different methanol molar fractions x in the liquid phase in equilibrium with the gas mixture fed to the photoreactor. Contributions of the oxidation paths: indirect path (dotted line); direct path (dashed-dotted lines) and water assisted path (dashed line). Reprinted from Ref. [44], Copyright (2011), with permission from Elsevier.*

Thus, as shown in Fig. 10, the rate results obtained in the vapor phase photocatalytic methanol reforming on noble metal modified TiO$_2$ at different methanol molar fractions were found to adequately fit a reaction scheme implying three parallel oxidation paths [44]: i) an indirect •OH radical-mediated path; ii) a direct path, implying the reaction of valence band holes with adsorbed methanol and iii) a water-assisted path.

3. Testing TiO$_2$-based photoelectrodes and membranes

The great majority of photocatalytic water splitting systems implies the evolution of a mixture of hydrogen and oxygen in only one reactor; of course a separation step would be required prior to any use of the hydrogen produced by this way. For this reason we set up and tested a two compartment Plexiglas cell for separate hydrogen and oxygen production from photocatalytic water splitting [45]. The two compartments of this cell are separated by a photoactive electrode surmounting a proton exchange Nafion membrane. As better detailed in Fig. 11, the photoelectrode consists in a thin titanium dioxide layer, acting as photoanode, deposited on one side of a titanium disk and a platinum layer, acting as cathode, deposited on the opposite side [46]. One of the two compartments of the cell is filled with a NaOH solution (side A, in contact with the TiO$_2$ film), the other one with a H$_2$SO$_4$ water solution (side B, in contact with the Pt film), in order to attain a small chemical bias. When side A of the cell is illuminated, water splitting into molecular oxygen (from side A) and hydrogen (from side B) occurs at constant rate. The evolved gases are collected in the two upside down graduated burettes surmounting the two cell compartments and their volume is determined.
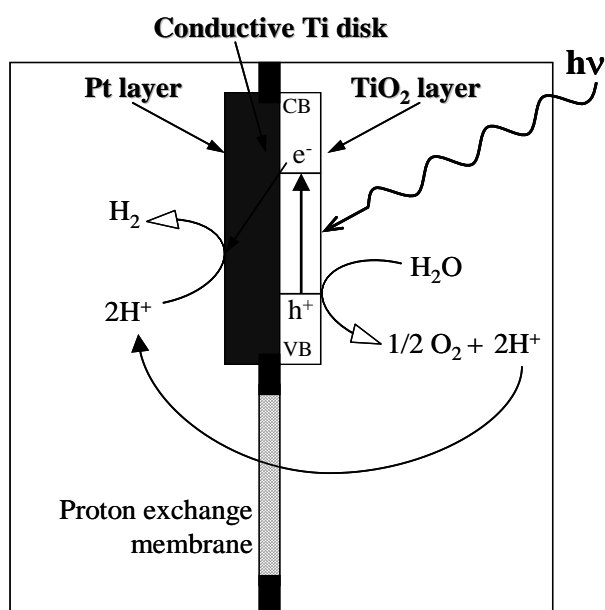

Fig. 11. *Detail of the photoelectrode placed in the wall separating the two compartments of the water photosplitting cell. Reprinted with permission from Ref. [46]. Copyright © 2010, Eureka Science Ltd.*

The first photoelectrodes for the cell were obtained by depositing the TiO$_2$ film by RF magnetron sputtering. When the titanium disk was kept at 450 °C during deposition, the so obtained films consisted of almost pure anatase, whereas the deposited TiO$_2$ mainly consisted of rutile, when the RF magnetron sputtering deposition was carried out with the titanium disk kept at 600 °C. Also in this case, rutile was found to be more active in hydrogen production, with respect to the anatase

18

phase [45], most probably as a consequence of the already mentioned superior ability of rutile to absorb longer wavelength light. More recent studies on the optimization of the photoanode for hydrogen production within the cell were carried out in comparison with incident photon to current efficiency measurements and revealed that the optimal TiO_2 film thickness was reached by a 6 h long RF magnetron sputtering deposition under our deposition conditions [47]. Longer deposition times produce thicker films with an increased probability of electron-hole recombination along the more extended electron path.

Electrochemical anodization followed by annealing was found to be an alternative, effective and easily tunable route to produce TiO_2 nanotubes (NTs) layers supported on large surface photoelectrodes (see Fig. 12), to be also employed as active materials in our two compartment photosplitting cell [48]. The anodization time length was found to be the key factor to produce well aligned and top-open NT arrays with an optimal aspect ratio. The photocatalytic activity of such TiO_2 NT arrays was perfectly paralleled by their performance in photocurrent measurements, indicating that both their photocatalytic and photoelectrochemical behavior largely depends on the NTs length and morphology.
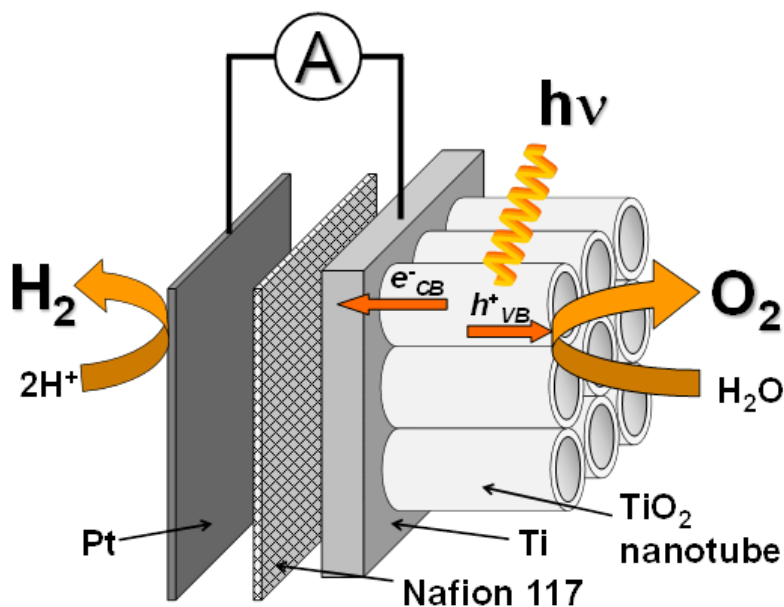
Fig. 12. *Sketch of the TiO₂ NTs photoelectrode showing the mechanism of separate H₂ and O₂ production through photocatalytic water splitting. Reprinted from Ref. [48], Copyright (2013), with permission from Elsevier.*

Such technique was further explored to produce Ta-doped [49] and Au-decorated TiO_2 NTs [50] or to produce self-organized arrays of single metal catalyst particles in TiO_2 cavities for highly

efficient photocatalytic systems [51]. All these systems were found to be effective for producing tailored photoelectrodes, to be employed for photocatalytic hydrogen production.

It is finally worth mentioning that photocatalytic hydrogen production by ethanol photo steam reforming was obtained also employing TiO_2-based photoactive membranes fabricated by supersonic cluster beam deposition on glass fiber filters [52]. The nanostructured TiO_2 and Pt/TiO_2 coatings produced by expanding flame-made powders in a supersonic beam consisted of crystalline nanoparticles (mainly anatase), without any need of post-deposition annealing. The rate of hydrogen production was found to increase with increasing Pt content in the photoactive material, up to 1.5 wt% Pt, with a better performance with respect to more conventional compact photocatalyst thin films tested in a flowing photoreactor.

4. Perspectives

In spite of the enormous efforts carried out all over the world in the last decade, the photocatalytic production of hydrogen seems to be still quite far from real large-scale production applications, essentially because the efficiency in light harvesting and charge separation of the up to now developed photocatalytic materials, in particular the TiO_2-based ones, is still too low. The main achievements attained so far consist in a quite extensive understanding of the processes at the basis of photocatalysis, which have been mainly obtained employing TiO_2-based photocatalysts, and in the continuous development of innovative semiconductor materials and technologies to produce them. Novel composite or functionalized photoactive materials, also containing efficient electron- or hole-trapping co-catalysts, as well as organic/inorganic hybrid systems and chemically different, low band gap, coupled new materials, are presently regarded as promising ways to achieve full solar light exploitation for hydrogen production from water. Sophisticated preparation techniques, able to control and tune the electronic properties of photocatalytic materials, would certainly also play a relevant role in the near future, together with time-resolved and space-resolved spectroscopic techniques in connection with computational investigations, which will provide more in depth information on electronic properties of photocatalytic materials, for their better tailored engineering.

References

[1] M. Ni, M.K.H. Leung, D.Y.C. Leung, K. Sumathy, Renew. Sustain. Energy Rev. 11 (2007) 401–425.

[2] A. Fujishima, X. Zhang, D.A. Tryk, Surf. Sci. Rep. 63 (2008) 515–582.

[3] A. Kudo, Y. Miseki, Chem. Soc. Rev. 38 (2009) 253–278.

[4]   M. Kitano, M. Hara, J. Mater. Chem. 20 (2010) 627–641.

[5]   F. Zuo, L. Wang, T. Wu, Z. Zhang, D. Borchardt, P. Feng, J. Amer. Chem. Soc. 132 (2010) 11856–11857.

[6]   Z. Zou, J. Ye, K. Sayama, H. Arakawa, Nature 414 (2001) 625–627.

[7]   Z. Zou, H. Arakawa, J. Photochem. Photobiol. A 158 (2003) 145–162.

[8]   H. Kato, A. Kudo, Catal. Today 78 (2003) 561–569.

[9]   R. Abe, M. Higashi, K. Sayama, Y. Abe, H. Sugihara, J. Phys. Chem. B 109 (2005) 16052–16061.

[10] W. Yao, J. Ye, Chem. Phys. Lett. 435 (2007) 96–99.

[11] J. Zhang, J. Yu, Y. Zhang, Q. Li, J.R. Gong, Nano Letters 11 (2011) 3026–3033.

[12] D. Wang, A. Pierre, G. Kibria, K. Cui, X. Han, K.H. Bevan, H. Guo, S. Paradis, A. Hakima, Z. Mi. Nano Letters 11 (2011) 2353–2357.

[13] A. Ishikawa, T. Takata, J.N. Kondo, M. Hara, H. Kobayashi, K. Domen, J. Amer. Chem. Soc. 124 (2002) 13547–13553.

[14] M. Higashi, K. Domen, R. Abe, J. Amer. Chem. Soc. 134 (2012) 6968–6971.

[15] Y. Ma, X. Wang, Y. Jia, X. Chen, H. Han, C. Li, Chem. Rev. 114 (2014) 9987–10043.

[16] X. Zou, Y. Zhang, Chem. Soc. Rev. 44 (2015) 5148–5180.

[17] S. Bai, W. Yin, L. Wang, Z. Li, Y. Xiong, RCS Adv. 6 (2016) 57446–57463.

[18] A.L. Linsebigler, G. Lu, J.T. Yates, Chem. Rev. 95 (1995) 735–738.

[19] P. Kamat, J. Phys. Chem. B 106 (2002) 7729–7744.

[20] Q. Gu, J. Long, L. Fan, L. Chen, L. Zhao, H. Lin, X. Wang, J. Catal. 303 (2013) 141–155.

[21] L. Fan, J. Long, Q. Gu, H. Huang, H. Lin, X. Wang, J. Catal. 320 (2014) 147–159.

[22] M. Maisano, M.V. Dozzi, E. Selli, J. Photochem. Photobiol. C: Photochem. Rev. 28 (2016) 29–43.

[23] J. Greaves, L. Al-Mazroai, A. Nuhu, P. Davies, M. Bowker, Gold Bulletin 39 (2006) 216–219.

[24] N. Strataki, V. Bekiari, D.I. Kondarides, P. Lianos, Appl. Catal. B: Environ. 77 (2007) 184–189.

[25] G. Wu, T. Chen, W. Su, G. Zhou, X. Zong, Z. Lei, C. Li, Int. J. Hydrogen Energy 33 (2008) 1243–1251.

[26] O. Rosseler, M.V. Shankar, M. Karkmaz-Le Du, L. Schmidlin, N. Keller , V. Keller, J. Catal. 269 (2010) 179–190.

[27] M. Kang, J. Molec. Catal. A: Chem. 197 (2003) 173–183.

[28] H. Yoshida, K. Hirao, J. Nishimoto, K. Shimura, S. Kato, H. Itoh, T. Hattori, J. Phys. Chem. C 112 (2008) 5542–5551.

[29] G.L. Chiarello, E. Selli, L. Forni, Appl. Catal. B: Environ. 84 (2008) 332–339.

[30] G.L. Chiarello, L. Forni, E. Selli, Catal. Today 144 (2009) 69–74.

[31] L. Mädler, W.J. Stark, S.E. Pratsinis, J. Mater. Res. 18 (2003) 115–120.

[32] G.L. Chiarello, I. Rossetti, L. Forni, J. Catal. 236 (2005) 251–261.

[33] W.I. Teoh, F. Denny, R. Amal, D. Friedmann, L. Mädler, S.E. Pratsinis, Top. Catal. 44 (2007) 489–497.

[34] G.L. Chiarello, M.H. Aguirre, E. Selli, J. Catal. 273 (2010) 182–190.

[35] M. Mrowetz, A. Villa, L. Prati, E. Selli, Gold Bulletin 40 (2007) 154–160.

[36] M.V. Dozzi, G.L. Chiarello, E. Selli, J. Adv. Oxid. Technol. 13 (2010) 305–312.

[37] G.L. Chiarello, A. Di Paola, L. Palmisano, E. Selli, Photochem. Photobiol. Sci. 10 (2011) 355–360.

[38] M.V. Dozzi, S. Livraghi, E. Giamello, E. Selli, Photochem. Photobiol. Sci. 10 (2011) 343–349.

[39] M.V. Dozzi, B. Ohtani, E. Selli, Phys. Chem. Chem. Phys. 13 (2011) 18217–18227.

[40] M.V. Dozzi, A. Saccomanni, M. Altomare, E. Selli, Photochem. Photobiol. Sci. 12 (2013) 595–601.

[41] M.V. Dozzi, C. D'Andrea, G. Valentini, B. Ohtani, E. Selli, J. Phys. Chem. C 117 (2013) 25586–25595.

[42] G.L. Chiarello, M.V. Dozzi, M. Scavini, J.-D. Grunwaldt, E. Selli, Appl. Catal. B: Environ. 160–161 (2014) 144–151.

[43] J.H. Liu, A.Q. Wang, Y.S. Chi, H.P. Lin, C.Y. Mou, J. Phys. Chem. B 109 (2005) 40–43.

[44] G.L. Chiarello, D. Ferri, E. Selli, J. Catal. 280 (2011) 168–177.

[45] E. Selli, G.L. Chiarello, E. Quartarone, P. Mustarelli, I. Rossetti, L. Forni, Chem. Commun. (2007) 5022–5024.

[46] G.L. Chiarello, E. Selli, Recent Patents on Engineering 4 (2010) 155–169.

[47] G.L. Chiarello, C. Tealdi, P. Mustarelli, E. Selli, Materials 9 (2016) 279.

[48] M. Altomare, M. Pozzi, M. Allieta, L.G. Bettini, E. Selli, Appl. Catal. B: Environ. 136–137 (2013) 81–88.

[49] M. Altomare, K. Lee, M.S. Killian, E. Selli, P. Schmuki, Chem. Eur. J. 19 (2013) 5841–5844.

[50] K. Lee, R. Hahn, M. Altomare, E. Selli, P. Schmuki, Adv. Mater. 25 (2013) 6133–6137.

[51] J.E. Yoo, K. Lee, M. Altomare, E. Selli, P. Schmuki, Angew. Chem. Int. Ed. 52 (2013) 7514–7517.

[52] F. Della Foglia, G.L. Chiarello, M.V. Dozzi, P. Piseri, L.G. Bettini, S. Vinati, C. Ducati, P. Milani, E. Selli, Int. J. Hydrogen Energy 39 (2014) 13098–13104.